

Review

UAS-Borne Radar for Remote Sensing: A Review

Lapo Miccinesi , Alessandra Beni  and Massimiliano Pieraccini 

Department of Information Engineering, University of Florence, 50139 Firenze, Italy

* Correspondence: lapo.miccinesi@unifi.it

Abstract: Since the 1950s, radar sensors have been widely used for the monitoring of the earth's surface. The current radars for remote sensing can be divided into two main categories: Space/aerial-borne and ground-based systems. The unmanned aerial system (UAS) could bridge the gap between these two technologies. Indeed, UAS-borne radars can perform long scans (up to 100/200 m) in a brief time (a few minutes). From the 2010s, the interest in UAS-borne radars has increased in the research community, and it has led to the development of some commercial equipment and more than 150 papers. This review aims to present a study on the state-of-the-art of UAS-borne radars and to outline the future potential of this technology. In this work, the scientific literature was categorized in terms of application, purpose of the paper, radar technology, and type of UAS. In addition, a brief review of the main national UAS regulations is presented. The review on the technological state-of-the-art shows that there is currently no standard in terms of radar technology, and that the multi-helicopter could be the most used UAS in the near future. Moreover, the UAS-borne radar can be used for several remote sensing applications: From landmine detection to smart agriculture, and from archeological survey to research and rescue applications. Finally, the UAS-borne radar appears to be a mature technology, which is almost ready for industrialization. The main developmental limit may be found in the flight regulation, which does not allow for many operations and imposes strict limits on the payload weight.

Keywords: radar development; radar technology; remote sensing; UAS-borne radar



Citation: Miccinesi, L.; Beni, A.; Pieraccini, M. UAS-Borne Radar for Remote Sensing: A Review. *Electronics* **2022**, *11*, 3324. <https://doi.org/10.3390/electronics11203324>

Academic Editor: Krzysztof S. Kulpa

Received: 5 September 2022

Accepted: 11 October 2022

Published: 15 October 2022

Publisher's Note: MDPI stays neutral with regard to jurisdictional claims in published maps and institutional affiliations.



Copyright: © 2022 by the authors. Licensee MDPI, Basel, Switzerland. This article is an open access article distributed under the terms and conditions of the Creative Commons Attribution (CC BY) license (<https://creativecommons.org/licenses/by/4.0/>).

1. Introduction

Unmanned aerial systems (UASs) are widely used for remote sensing applications. The use of UAS allows for the development and production of flexible systems that could be operated in several scenarios and critical situations, and could cover large areas with cost-effectiveness. Currently, most of the payloads (additional sensors for UAS applications) are based on optical/multispectral sensors. These sensors are particularly suitable for integration in UAS systems, as they are already designed for remote operation. Moreover, the metadata (position and time) could be easily embedded in the raw data. These types of sensors have been the subject of several scientific reviews in the last few years [1–7]. In 2012, Zhang et al. published a review on UAS for precision agriculture [1]. In 2014, Colomina et al. presented a review on photogrammetry for remote sensing using UAS [8], and in 2019, Manfreda et al. addressed the problem of the use of UAS for environmental monitoring [2]. Finally, Vélez-Nicolás et al. presented a review on the application of UAS for hydrological issues [7]. Some of these reviews suggested that the survey should be performed using a radar, which has several advantages, such as longer operating range and insensitivity to light and visibility conditions. In the present review, we examine in depth both the technical development and the possible applications of UAS-borne radars. In fact, the radar payload is currently a mature technology; however, it is not ready for commercialization with respect to the payloads covered in the aforementioned reviews (optical, multispectral sensors) [1–8].

The current radar systems for remote sensing operate onboard of an orbiting/flying system (satellite or aerial) or using a terrestrial platform [9,10]. The satellite/aerial-borne

radar can monitor large areas and perform high-resolution images. On the one hand, these systems have long return times: A satellite system takes days to overlook the same area from the same direction. On the other hand, terrestrial systems cover smaller areas (from building to a single slope) with a return time in the order of minutes.

Since 2006, unmanned aerial systems (UASs) have been studied as platforms for radar remote sensing [11]. The UAS-borne radar could bridge the gap between satellite/aerial and terrestrial systems, as schematically shown in Figure 1. UAS-borne radars could cover larger areas with respect to terrestrial systems, with a shorter return time. These two characteristics, combined with the flexibility of UAS systems, allow for the use of UAS in different applications, such as landmine detection [12], snow/ice monitoring [13], deformation measurement [14], and biomass survey [15].

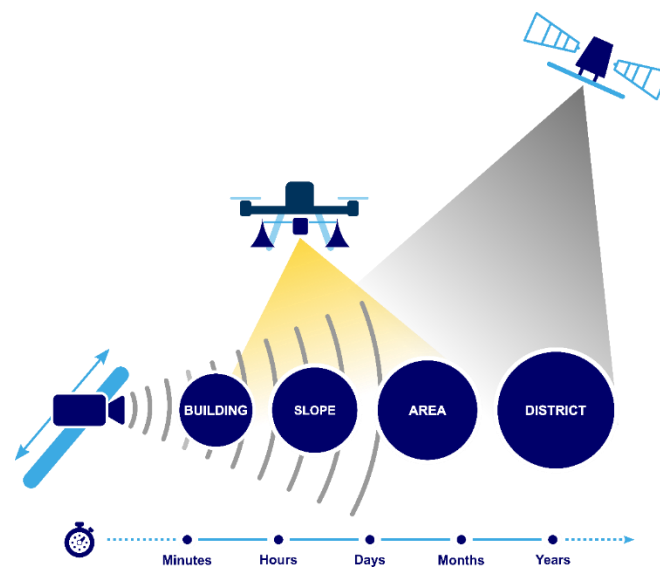


Figure 1. Complementarity of UAS-borne radar with terrestrial and spaceborne systems.

Compared to conventional systems, the UAS radar can be deployed within minutes and used in scenarios where ground systems cannot be operated. For example, a UAS-borne radar can be used for landmine detection, since it operates with no contact on the surface. Moreover, it can be used in areas where the ground line-of-sight is covered by obstacles, such as wooden or urban areas. Furthermore, it can be used in emergency situations in cooperation with other payloads.

On the other hand, the UAS trajectory is commonly less precise than other conventional systems, and it could dramatically affect the image quality. The uncertainty on the trajectory is particularly evident when the operator needs to retrace the same path, for example, in interferometric applications or for image correlation. The flight uncertainty is related to two factors: The intrinsic uncertainty of positioning and inertial sensors, and the constraints related to the flight controller systems. Furthermore, with respect to conventional systems, the operations with UAS are limited by the weather conditions, i.e., wind dramatically affects the flight performance, and generally flying is not possible under raining conditions.

The principal characteristics of spaceborne, terrestrial, and UAS-borne radars are compared in Table 1. The main drawbacks of UAS-borne systems are related to autonomy (between 20 and 50 min) and the operating limits related to the weather. Indeed, most of the UAS could not be operated in adverse weather conditions (wind, rain, etc.). On the other hand, the advantages are the short return time, the coverage area, and the resolution which is a tradeoff between spaceborne and terrestrial systems.

Table 1. EASA pilot certificate's category, limitations, and UAS requirements.

	Spaceborne	Terrestrial	UAS-Borne
Autonomy	∞	∞	20/50 min
Weather condition operativity	Operative in each weather condition	Operative in each weather condition	Could not be operated in each weather condition
Return time	Days	Minutes	Minutes–hours
Resolution	Constant with the range (spatial resolution)	Function of range (angular resolution)	Constant with range or angles depending on operative modality
Coverage	Global	1 km ²	10 km ²

The UAS-borne radar appears to be a mature technique for remote sensing, and it is almost ready for industrialization. However, a systematic study of UAS-borne radar in terms of radar technology and remote sensing applications has not yet been performed. The aim of this review is to provide a comprehensive overview of UAS-borne radars. Specifically, in this paper the technical aspects, such as signal modulation, operative band, and imaging techniques, and the main applications of UAS-borne radars are extensively reviewed and discussed.

Moreover, we summarize the national flight regulations that involve UAS systems. Since the last 5 years, several countries have legislations on UAS operations. These regulations must be considered by both the developer and the user. In fact, they involve the mass of the payload and the areas where it is possible to operate the UAS.

The present review paper is structured as follows. In Section 2, we describe the methods used for the bibliographic research and for categorizing the papers. In Section 3, we address the main national regulations of the UAS. In Section 4, we recall the working principle of radars and the main processing techniques. Then, we summarize the results of the bibliographic review in terms of radar technologies. In Section 5, the main UAS-borne radar applications for remote sensing are summarized. In Section 6, we discuss the results and the future of UAS-borne radars in terms of radar developments and applications. Finally, Section 7 contains final considerations regarding the current UAS regulation and its implications for the use of these systems.

2. Methods

The present review aims to study the current state-of-the-art of UAS-borne radars for remote sensing and to outline its potential in terms of technologies and applications. The study on the state-of-the-art was carried out by considering 162 papers found in the main online databases: Google Scholar, Scopus, and Web of Science. The keywords used were a combination of drone, GPR, imaging, radar, synthetic aperture radar, UAS, and UAV (alphabetic order). The papers were categorized in terms of radar technology, imaging technique, type of UAS, and application.

In the present review, we considered open access materials (articles, conference papers, books, etc.) and those subscribed by the University of Florence. The excluded papers were less than 10% of the total and the majority were conference papers. We excluded pre-print papers, for example, those presented in arXiv but not published by an editor. Furthermore, we excluded papers on military applications, as they were out of the scope of this review.

The papers were collected using Zotero [16] and classified in a spreadsheet document in terms of (but not limited to) signal modulation, operative band, imaging technique, type and antennas configuration, type of UAS, take-off weight, generic and specific applications. The classification was performed paper by paper without machine techniques or automatic tools. For the review, we also considered papers that addressed a proof of concept or papers where the authors designed a specific radar component (antennas, transceiver, positioning system) for improving an existing prototype. We discarded papers that focused on the use of the radar as an ancillary system, not aboard of the UAS.

Results have been synthesized by counting the number of papers for each category and reporting them in a graph or percentage form. The percentage was calculated using a normalization factor that considers the number of papers for each diverse application.

As for the review of national regulations (Section 3), we used the national aviation portal of many countries and a site aggregator [17], which collects and resumes the national regulations of several countries.

Figure 2 shows the number of papers per year, except for a preliminary work in 1996 [18] where Vesecky and Cornwall addressed the problem of power consumption, without proposing any practical system. The first prototype has been presented by Zaugg et al. [11] in 2006, which has been developed by a group of students at Brigham Young University, Provo, UT, US. From 2016, the number of papers that were published has increased, which is possibly related to the introduction of commercial multi-copter (commonly named the drone). The number of publications appears to have remained stable from 2016 through the present time.

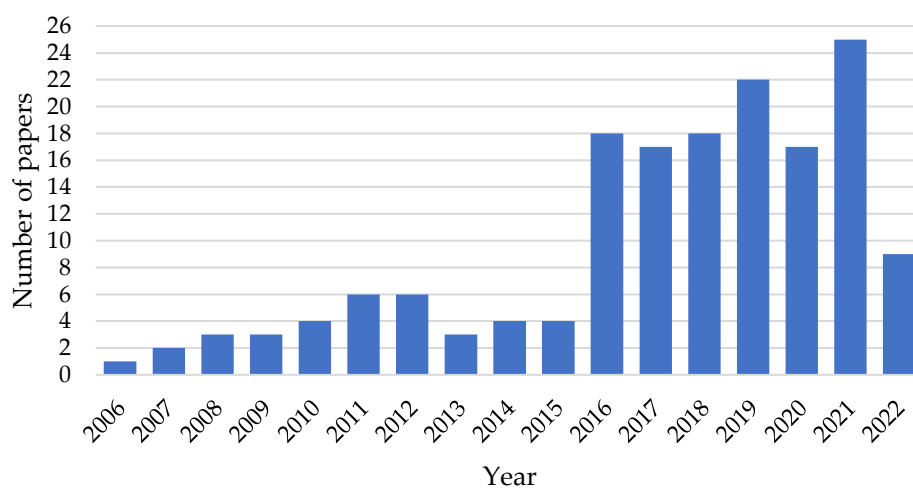


Figure 2. Number of papers per year.

3. Review of International UAS Regulations

For a certain number of countries, there are specific regulations for the use of UAS due to their increasing number. Currently, the national regulations are non-homogeneous, but there are some common policies. These policies pose constraints on the work of the payload designer and place limits on the final technical users.

In general, the maximum take-off weight (MTOW) of the UAS for hobby or professional use must be lower than 25 kg. Moreover, in many countries, it is compulsory to register the UAS with national aviation authorities and every pilot must have a certificate to be able to operate the UAS (Europe, China, India, etc.) [19–23]. Meanwhile, in some countries, the certificate is compulsory only for professional use [24]. In summary, the principles of risk assessment and possibility of use are at the basis of each country's regulations.

Briefly, we herein reported on the regulation of the European Union as an example of the trade-off between risk assessment and possibility of use. The European Union unified the regulation for each country's members toward the European Union Aviation Safety Agency (EASA) regulation 2019/947 [19]. Each UAS must be registered in a national registry and, from 2024, must be equipped with a transponder for remote identification.

The use of UAS is defined in terms of risk assessment, as shown in Figure 3. The flight of the UAS could be at the maximum altitude of 120 m in an open category (minimum risk), with a distance from un-involved people or buildings regulated by the pilot certificate (A1/A2/A3). The flight must be performed in a visual line-of-sight modality. All other cases (exceeding the maximum altitude, flying near people or infrastructures, beyond line-of-sight) require a specific certificate and a specific risk assessment (SORA). Furthermore, flying in a controlled airspace requires a specific certificate.

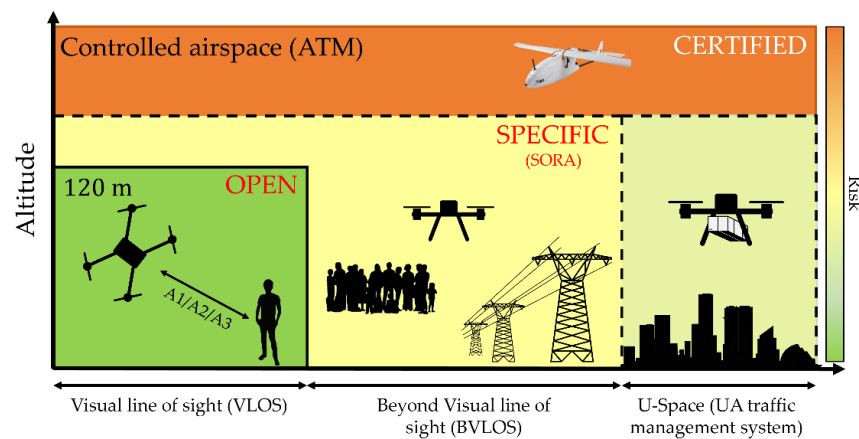


Figure 3. Scheme of UAS regulation in terms of altitude, distance from the pilot, and risk assessment.

Both hobby and professional users can operate the drone in the open category by obtaining a pilot certificate. A brief scheme of rules of the open category is reported in Table 2. Of note, there is a relation between the MTOW (UAS requirements) and the subcategory limitations. Every UAS within 250 g and 4 kg can fly close to un-involved people and buildings, while the UAS over 4 kg has to be operated at a distance from people and buildings.

Table 2. EASA pilot certificate’s category, limitations, and UAS requirements.

Cat.	SUBCATEGORY LIMITATION	UAS REQUIREMENTS
A1	Overflight of UAS is permitted over people outside of an operation. Flying close to a populated area is allowed.	Private construction < 250 g and < 19 m/s Type C0 (<250 g) Type C1 (<900 g, e-ID, and Geo-awareness)
A2	Flying is allowed near people outside of an operation by maintaining a safety distance of 5–30 m. Flying close to a populated area is allowed.	Type C2 (<4 kg with low speed, e-ID, and Geo-awareness)
A3	Operation in areas where people are outside of an operation are not endangered by maintaining a minimum safety distance of 150 m from any populated area.	Private construction < 25 kg Type C2 (<4 kg, e-ID, and Geo-awareness) Type C3 (<25 kg, e-ID, and Geo-awareness) Type C4 (>25 kg)

The limits on the MTOW, and then on the payload, are challenging for the developer. Indeed, the developer of UAS-borne radar must pay attention to the total dimensions of the payload both in terms of weight and size.

4. Radar Technology

A large number of papers have been dedicated to radar developments both in terms of hardware and algorithms: More than 35% of the publications addressed radar development, 25% addressed imaging algorithms, and 17% feasibility studies. This percentage highlights the tight relation between UAS-borne radar and technological development.

In this section, we briefly resume the main radar principles. This can be useful to better understand the common issues related to the development of UAS-borne radar. Specifically, the main radar signal modulations, operative bandwidths, and imaging processes are reported, and their use is discussed.

4.1. Radar Signal Modulations

The radar can detect a target in its field of view by sending and receiving an electromagnetic signal. It measures the distance of a target (R_0) by measuring the delay (Δt) between the transmitted and received signal. The target distance can be calculated as follows:

$$R_0 = \frac{c \cdot \Delta t}{2}, \quad (1)$$

where c is the speed of light.

The range resolution, ΔR , (capability of discriminating two equal targets in range) is given by:

$$\Delta R = \frac{c}{2B}, \quad (2)$$

where B is the bandwidth.

The main signal modulations are shown in Figure 4. The first image (Figure 4a) represents a pulsed modulation: The transceiver sends a single pulse and measures the delay between the transmitted and received signal. Figure 4b schematically shows a continuous wave stepped frequency (SFCW) modulation. In this case, the transceiver sends a sweep of frequencies by holding each tone for a period of time. The continuous wave frequency modulated (FMCW) signal is shown in Figure 4c. In the FMCW modulation, the frequency changes linearly in time, and the distance is measured by considering the frequency difference between the transmitted and received signal. The main advantages of the different modulation are reported in [25].

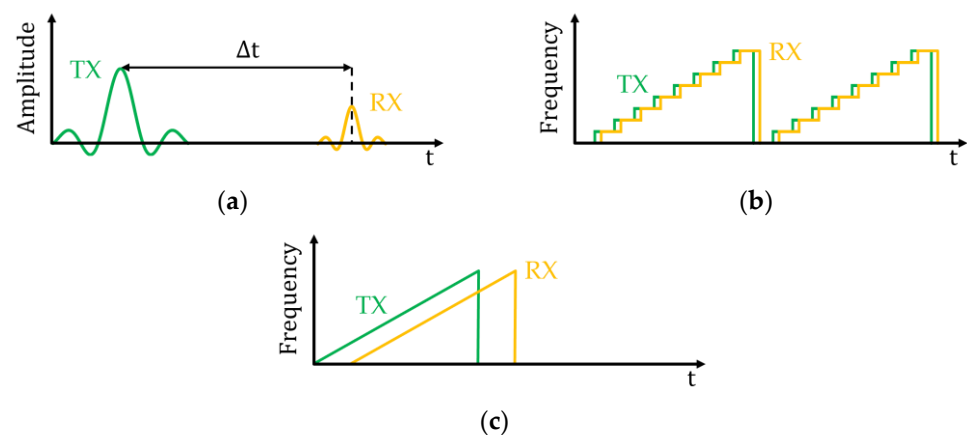


Figure 4. Radar signals: (a) Pulsed, (b) continuous wave stepped frequency (SFCW), (c) continuous wave frequency modulated (FMCW).

Figure 5 summarizes the number of papers in terms of signal modulation. For UAS applications, the FMCW is the most used (63% of papers), followed by pulsed equipment (18%), and finally SFCW (2.5%). In [13,26,27], Jessen et al. used a pseudo noise transceiver, which is an advanced modulation technique usually used for military purposes since it is more robust against the interference (it cannot be easily intercepted or jammed). Moreover, the authors selected this modulation due to a flatter amplitude inside the transmitted bandwidth, and a higher duty cycle.

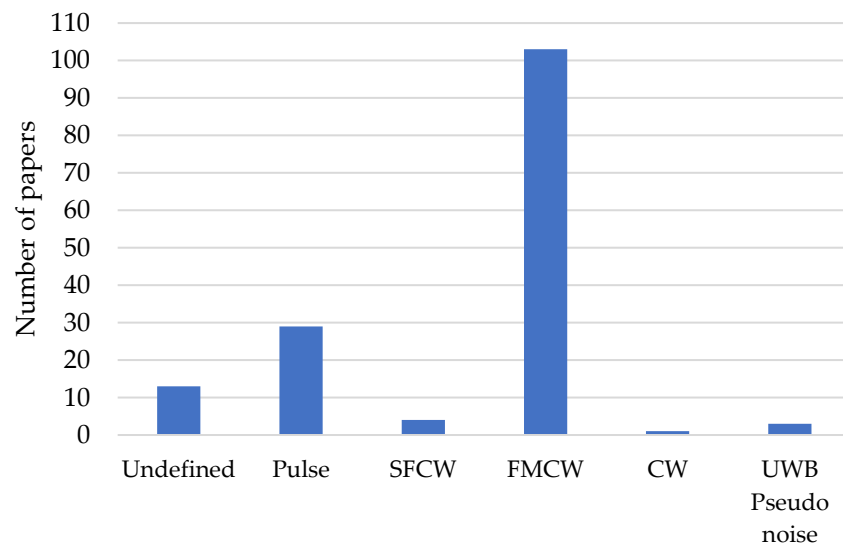


Figure 5. Number of papers in terms of radar signal.

A radar can obtain images by rotating the beam (mechanical or electronically) or by exploiting the movement of the platform. The first method is rarely used in UAS due to the weight and complexity of the hardware. The second method is more common, especially in combination with synthetic aperture radar (SAR) processing.

SAR exploits the movement of antennas in a direction perpendicular to the range as illustrated in Figure 6. During the flight, the radar continuously sends and receives an electromagnetic signal from the environment and exploits the movement of the UAS to perform the image. After a range compression, the single sweeps can be combined to achieve the azimuth resolution.

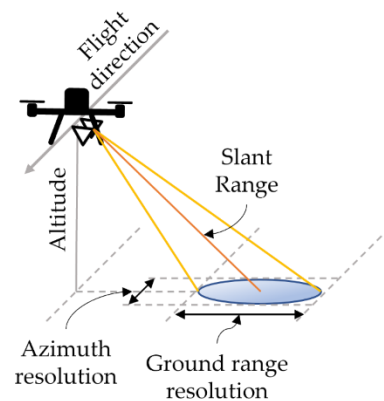


Figure 6. Radar imaging principle.

The azimuth resolution depends on the algorithm used for combining the sweeps and the distance between two consecutive sweeps, as shown in Figure 7.

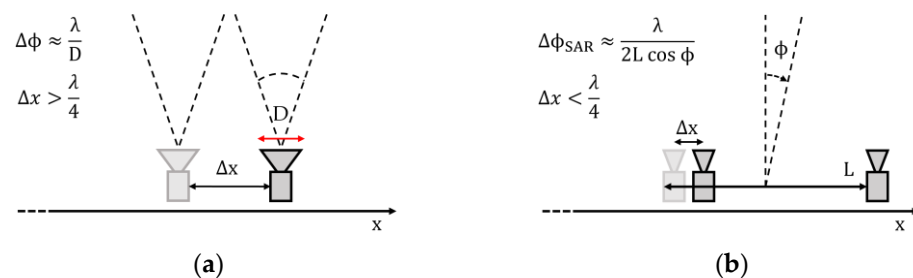


Figure 7. Azimuth resolution without azimuth compression (a) and for the SAR system (b).

If the consecutive signals are combined without any coherent summation along the flight direction, the azimuth resolution, $\Delta\phi$, is inversely proportional to the antenna aperture, D (Figure 7a):

$$\Delta\phi \approx \frac{\lambda}{D}, \tag{3}$$

where λ is the central frequency wavelength of the signal. Therefore, the physical aperture of the antennas limits the resolution, especially for the UAS-borne radar. In fact, the payload and holonomic constraints (i.e., the constraints related to the flight dynamic, such as the steering angle) places a limit on the physical dimension of the antennas.

SAR processing allows for the enhancement of the azimuth resolution, as shown in Figure 7b. In this case, to allow for a coherent summation, the distance between two consecutive antenna positions must be lower than:

$$\Delta x = \frac{\lambda}{4 \sin(\vartheta/2)}, \tag{4}$$

where $\vartheta = \lambda/D$ is the physical antenna aperture. Under this hypothesis, the azimuth resolution of a SAR system can be:

$$\Delta\phi_{\text{SAR}} \approx \frac{\lambda}{2L \cos \phi}, \tag{5}$$

where ϕ is the azimuth angle of the target, and L is the length of the aperture. In the limit of $L \ll R$, with R as the range of the target and $\phi \ll 1$, the azimuth resolution is theoretically equal to $\Delta x \sim D/2$.

The SAR method requires the calculation of a coherent sum along the scan direction, using a focusing algorithm. For UAS applications, back propagation algorithms are more suitable. These algorithms perform a coherent summation along the azimuth direction, by considering the relative distances between the UAS position and any point of the environment, as shown in Figure 8. The UAS trajectory is not an a priori parameter, but is known only after the flight. The final trajectory depends on the UAS dynamics, the flight controller, and on external factors, such as the wind. Usually, the user can define a trajectory using the software provided by the manufacturers. The flight controller uses this trajectory as a reference and changes the path fr time to time in order to compensate for the variations due to external factors, considering the holonomic constraints of the UAS.

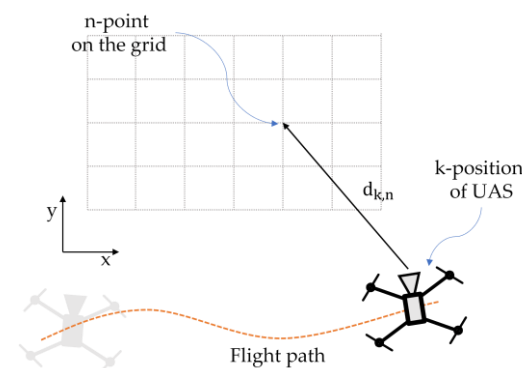


Figure 8. Focusing algorithm principle.

Since the position of UAS is used for obtaining the image, its accuracy should be roughly $\lambda/8$ or lower for obtaining the best performances. The accuracy of the position is related to the accuracy of the positioning system, which is usually within a meter using a global positioning satellite system (GNSS), and a few centimeters using a real-time kinematic (RTK-)GNSS. Few authors used the external positioning system, such as total

station [28] or laser meter as an altimeter [26,29,30], but they are an exception rather than the rule.

Moreover, advanced methods known as autofocus algorithms exist, which can compensate for the low accuracy of the position. In Section 4.3., we discuss in detail the results of the bibliographic review as related to these algorithms.

4.2. Operative Band

The operative band is a key parameter of a radar. By increasing the operative band, the range resolution increases. At the same time, the uncontrolled movements of the UAS could affect the image quality. The uncontrolled movements can be compensated as described in Section 4.1. The higher the frequency, the more sensitive the data are to the uncontrolled movement. The uncontrolled movement could affect the image quality, especially when the accuracy of telemetry sensors is larger than $\lambda/8$. Therefore, for high frequencies, an accurate motion compensation is required.

Figure 9 shows the percentage of papers for each operative band. The C- and L-bands are the most used bands, respectively, 19% and 17% of the papers. This result is related to the main applications of UAS-borne radar: The synthetic aperture radar and the ground penetrating radar. For SAR applications, the higher the frequency, the higher the resolution, but the effects of motion of the UAS are larger. The C-band represents a good trade-off between these two effects. In fact, the maximum accuracy achievable by the UAS sensor is in the order of 20/50 mm (using, for example, an RTK-GNSS). The wavelength in the C-band is within 37.5 and 75 mm, as compared to the accuracy of the positioning system. Moreover, the L-band has been used for SAR applications (16% of UAS-borne SAR systems have used the L-band against 19%, which have used the C-band). Of note, since focusing algorithms do not depend on the absolute position accuracy, the accuracy requirement can be relaxed by reducing the length of synthetic aperture.

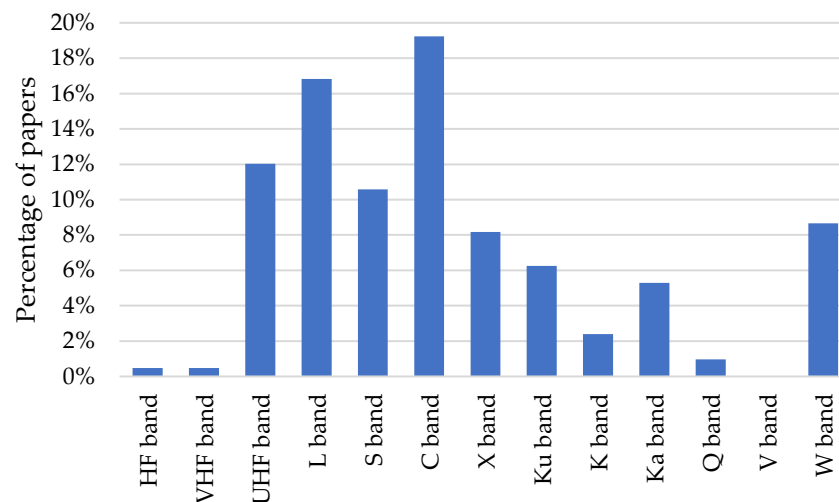


Figure 9. Number of papers in terms of operative bandwidth.

On the one hand, the GPR applications need a lower frequency to achieve a deeper penetration depth. On the other hand, the lower the frequency, the larger (and heavier) the equipment. In this case, the trade-off has been reached using UHF and the L-band.

The use of W-band is of particular interest. This operative band has recently been used for remote sensing applications, as radars operating in the W-band can be easily integrated on the UAS payload. This category is designed to be embedded in a single chip, which makes the payload particularly light. Moreover, the pulse repetition frequency (PRF) of this radar is usually remarkably high (few kHz) compared to the wavelength and average speed of UAS (few meters per second). Examples of the W-band radar can be found in [31–33].

4.3. Imaging Method

UAS-borne radars present a new challenge to the imaging method. Compared to conventional systems, the position accuracy is lower. Moreover, the UAS altitude is not constant during the flight, in particular for multi-copter systems. To overcome these problems, sophisticated imaging algorithms have been developed as described in Section 4.1.

For UAS applications, we can outline three methods: (1) Only altitude compensation, without azimuth compression; (2) back propagation algorithm, which considers the position of the UAS from time to time; (3) advanced method that uses autofocusing techniques. Figure 10 shows the percentage of papers for each imaging method.

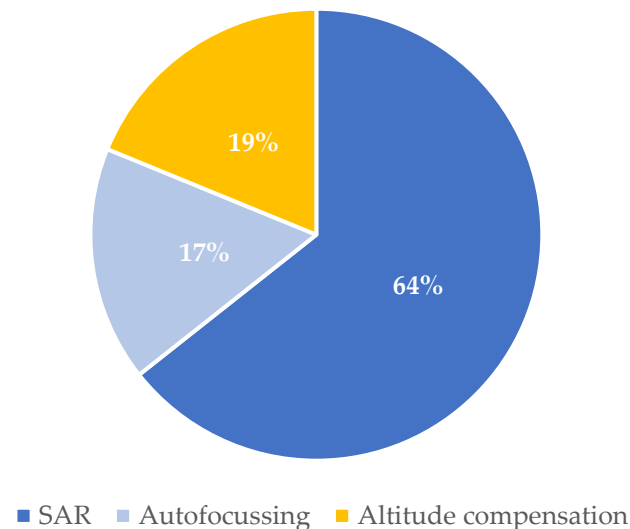


Figure 10. Percentage of the paper in terms of imaging method.

Figure 11 shows an example of only altitude compensation without azimuth compression [34]. The altitude compensation can be exploited by assuming that the ground is planar and horizontal. The altitude from the ground can be measured by telemetry [15], using the radar itself [34] or with an external sensor (for example, a laser meter) [13,26]. The result of the altitude compensation can be observed in Figure 11b, the ground appears horizontal, and the targets are more visible than Figure 11a. After altitude compensation, the radar image can be interpolated along the path (slow time in Figure 11) by considering the position of UAS from time to time [35,36]. In this case, the target can be associated with a physical coordinate in the environment.

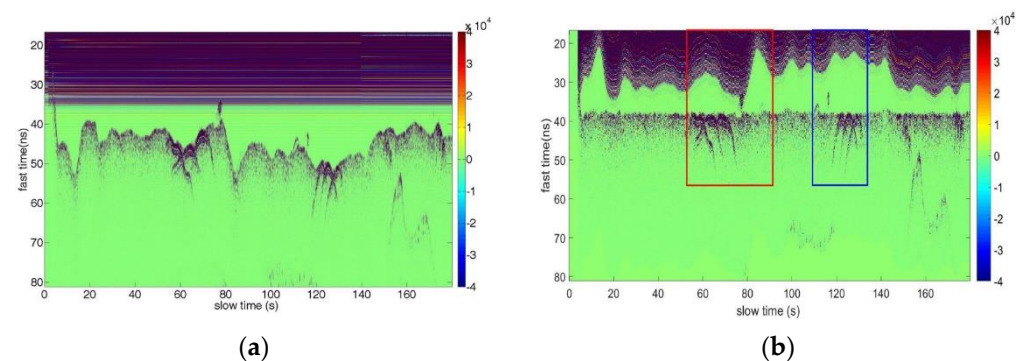


Figure 11. Example of altitude compensation (after [34]): (a) Before compensation, (b) after compensation.

The altitude compensation is usually used in cases where a high-resolution image is not necessary, for example, for measuring the gap between two media. Jessen et al. [13,26] used this method for measuring the depth of the snow cover, whereas Chen et al. [15]

estimated the forest profile. In [37], Ye et al. exploited the altitude compensation for a pseudo 3D map of the environment. The authors performed a scan of a planar surface with a MIMO radar to retrieve a bidimensional image (after altitude compensation). While the antennas were parallel to the surface, they sliced the horizontal image in terms of range to have a bidimensional map of the environment at different altitudes.

The SAR technique is the most used in UAS-borne radar applications. Considering the GPR application, about 70% of publications exploited this technique. In a large number of papers, the focusing algorithm is derived by a conventional back propagation algorithm [38]. The position of the UAS is usually retrieved from inertial sensors and GNSS. The most advanced UASs are equipped with RTK-GNSS systems, which increase the accuracy of the position. Few authors exploited other systems to retrieve the position of the UAS. For example, in [39], Schartel et al. integrated the RTK-GNSS data with the data from a terrestrial total station. Patel and Ferguson [28] used a light detection and ranging (LiDAR) system with an extended Kalman filter to retrieve the position of the payload during the flight.

The trajectory shape is the key point for SAR techniques. The conventional spaceborne and GB-SAR exploit the movement along a trajectory that can be considered almost linear. Recently, for GBSAR, a circular trajectory was used in the horizontal plane to enlarge the field of view [38,40,41] or a circular aperture was used in the vertical plane to measure the displacement vector [42]. For UAS-borne SAR, the linear aperture is one of the most used trajectories (Figure 12a) [29,43,44], even if, for particular applications, it is a landmine detection, the circular aperture has been used [45–49] (Figure 12b). Moreover, the UAS-borne SAR could exploit multiple-scans during the same flight as shown in Figure 12c. The multiple-scan survey not only increases the signal to noise ratio, but also the probability of detection of targets. Indeed, the radar cross section depends on the incident angle and on the specific radar-target position, especially for a complex target. The multi-scan is usually used for critical applications, such as landmine detection [12,50–52] or for rescue purposes [53].

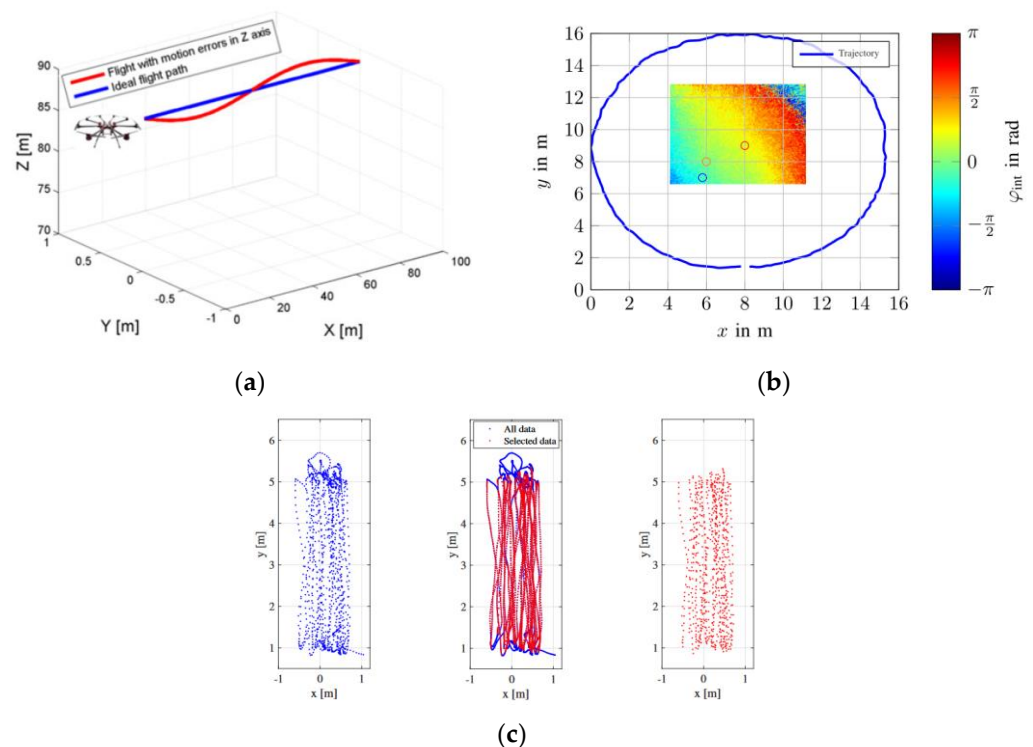


Figure 12. Examples of possible trajectory for UAS-borne SAR: (a) Linear scan (after [54]), (b) circular trajectory (after [47]), and (c) multi-scan (after [51]).

The autofocusing algorithm is a specific strategy of the back propagation method, which overcomes the problems due to non-compensated uncontrolled movements. These algorithms are particularly useful for UAS-borne SAR, when the position measured by the UAS is significantly noisy or corrupted for the retrieval of an image. An example of an autofocus algorithm application on UAS-borne SAR imaging is shown in Figure 13. Autofocusing algorithms usually perform an iterative optimization of a particular function to minimize the phase error and achieve a higher quality image. Several types of autofocusing algorithms exist, depending on the function to be optimized. One of the most used for SAR imaging is the phase gradient autofocus (PGA) [55], which is usually performed on strong scatterers on the imaged scene. The so-called phase gradient function is estimated and optimized by slightly changing a phase error term. In other cases, other types of cost functions are used, for instance, based on the integrated sidelobe level ratio [56] or on the signal entropy [57]. In the case of back propagation algorithms, the optimization can be performed by iteratively modifying the error trajectory [56].

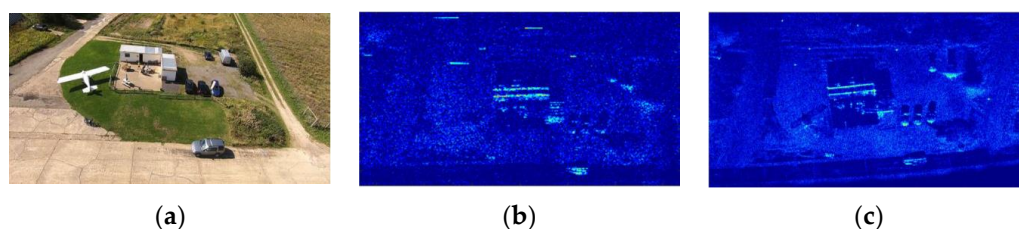


Figure 13. Examples of autofocusing algorithm (after [43]): (a) Optical image, (b) image without movement compensation, and (c) after movement compensation.

Autofocusing algorithms represent a powerful tool for obtaining high resolution SAR images even when there is a lack of information on the UAS trajectory. For instance, the authors of [43] presented an imaging method which exploits PGA techniques to achieve high-resolution images without the use of an on-board dedicated inertial navigation system. In [58], an autofocus framework for UAV-based UWB SAR data is presented. A weighted PGA is used to solve the local motion error estimation problem with frequency-dependent phase errors, and a trajectory deviation estimation is performed. Finally, the authors of [59] used autofocus techniques to compensate for the platform motion errors of a miniaturized, low-cost Ka-band UAS-borne SAR imaging system, which makes no use of motion sensors.

5. Remote Sensing Applications

In terms of applications, we can single out two main categories: Synthetic aperture radar (SAR) and ground penetrating radar (GPR). A residual number of papers do not address SAR and GPR applications. In these papers, the authors used only altitude compensations for generic applications. The most notable of these papers are reported in Section 4.3. Figure 14 shows the number of papers in terms of a specific application divided into three categories. The applications in SAR category varied in different fields, from agriculture to vital sign detection. Most of these papers have not declared the specific application and have been summarized in “remote sensing” applications. In the GPR category, most of the papers addressed the landmine detection.

Figure 15 shows the number of papers per year for each category. The blue dashed line represents the total number of papers. Until 2015, SAR was the main application, and from 2016, the interest in GPR applications increased.

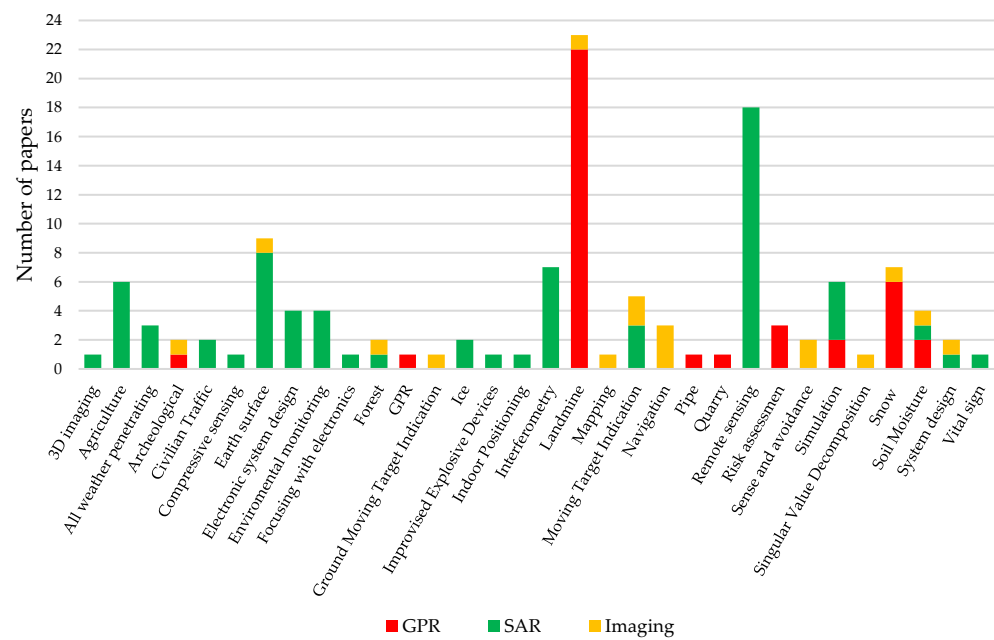


Figure 14. Number of papers per year in terms of specific applications.

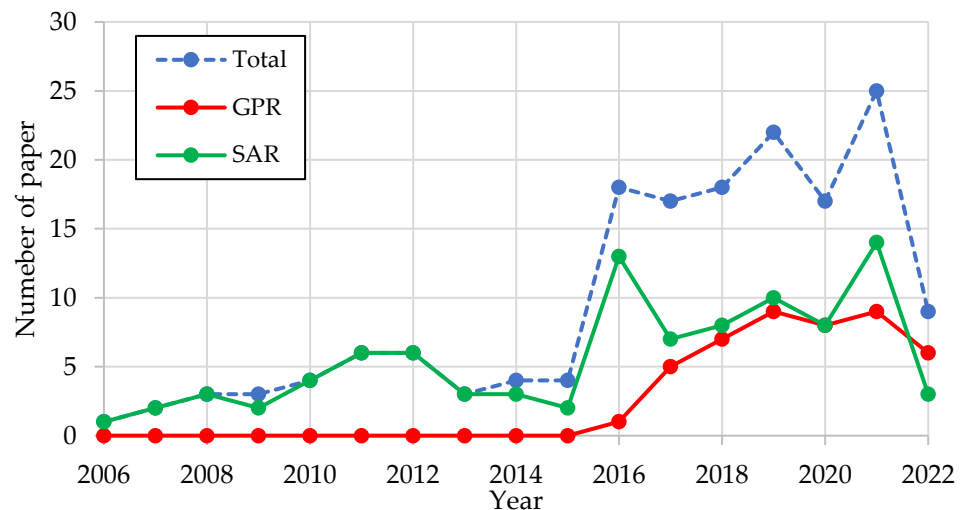


Figure 15. Number of papers per year: The blue dashed line shows the total number of papers, the green line shows the papers with SAR application, and the red line shows the papers with GPR application.

The peak in the number of papers in 2016 could be caused, not only by a greater interest in GPR, but also by the introduction of a novel class of UAS, the multi-copter. Since 2016, the total number of papers that used the multi-copter were five (including 2016), with respect to twenty-five papers that used fixed wing UAS. As shown in Figure 16, there are two main UAS categories: The fixed-wing (Figure 16a,b) and multi-copter (Figure 16c–e). The fixed-wing UASs are commonly used for covering large areas, and they can carry a heavier payload with longer flight duration. On the one hand, they are characterized by poor maneuverability (they can cover rectilinear trajectories). On the other hand, the multi-copters are characterized by high maneuverability (in terms of piloting and trajectory). The main drawbacks of the multi-copters are the MTOW (usually lower than 15 kg) and the flight duration (usually within 10 and 50 min).

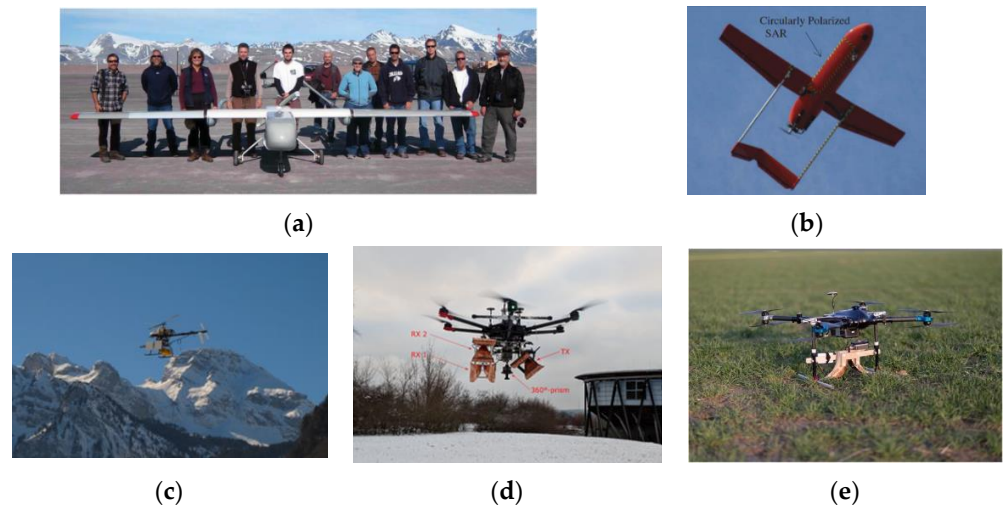


Figure 16. Examples of types of UAS: Fixed-wing (a) (after [60]) and (b) (after [61]); and multi-copter (c) (after [14]), (d) (after [45]), and (e) (after [62]).

Figure 17 shows the percentage of papers per year related to a specific UAS category. The sum of the percentage of paper per type is not always 100% since in some papers, the authors have not declared the type of UAS used. We can notice an inversion between fixed-wing and multi-copter in 2016. Before 2016, nearly all of the publications used a fixed-wing equipment, but from 2016, most of the papers (about 60%) used a multi-copter system, while only 5/6% of papers used the fixed-wing system. Generally, multi-copters are more versatile for most of the applications. In addition, multi-copters are designed to be compatible with a large number of different payloads, thus they are particularly suitable for research purposes.

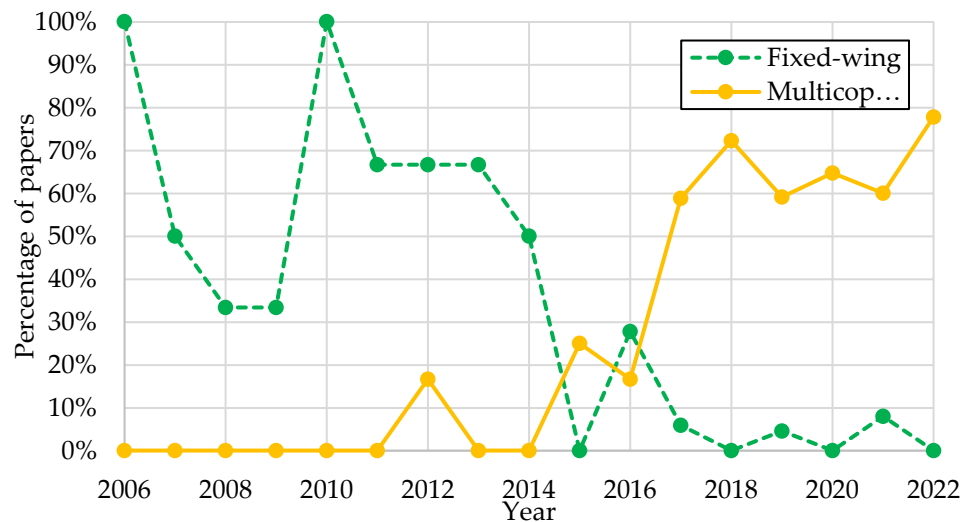


Figure 17. Type of UAS per year.

5.1. Synthetic Aperture Radar

The applications of UAS-borne SAR extend from generic earth monitoring [31,63–65] to more specific applications, such as interferometry [14,66–69], agriculture [70–73], moving target identification [74,75], and vital sign detection [76]. Figure 18 shows some examples of these applications.

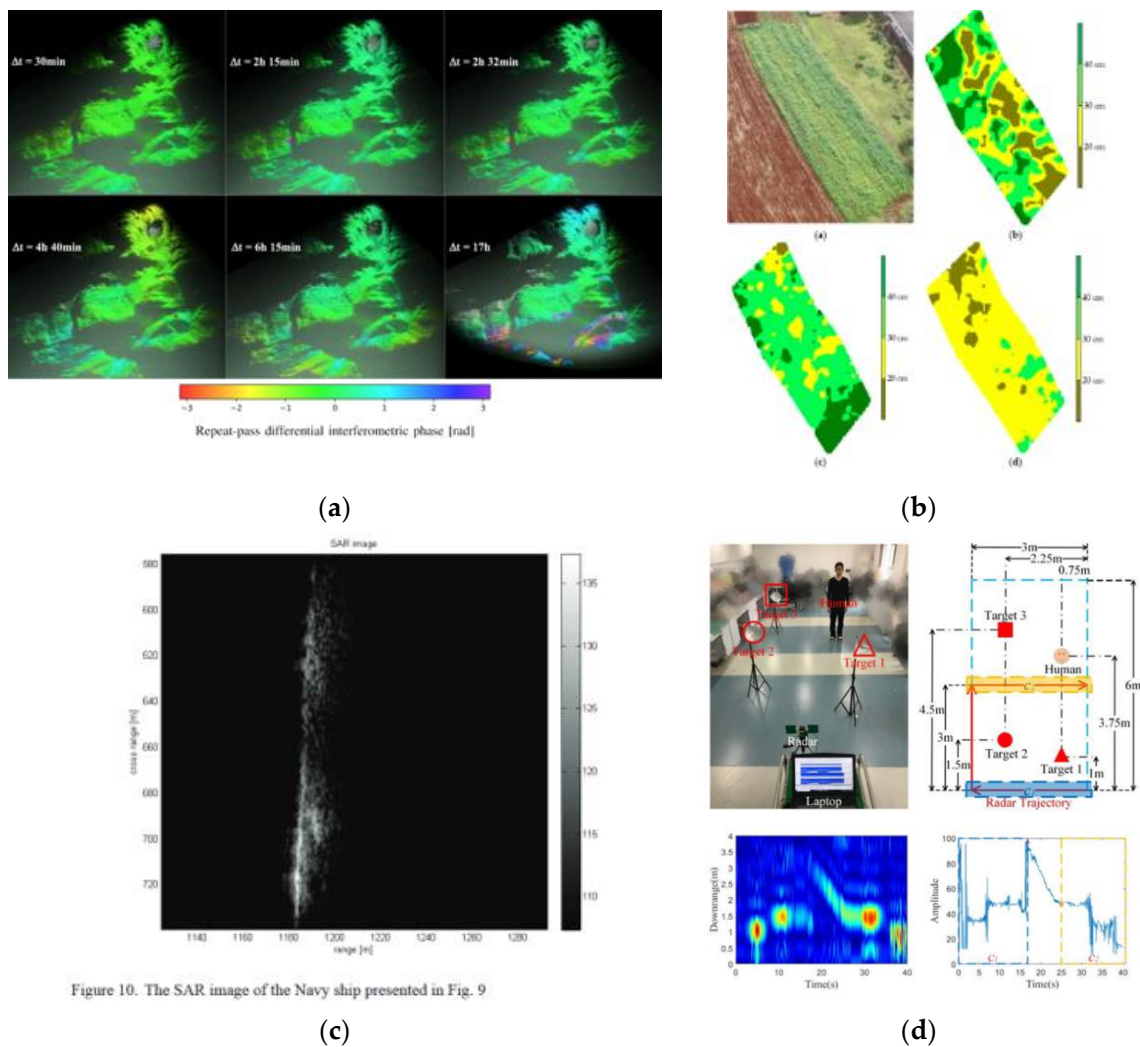


Figure 10. The SAR image of the Navy ship presented in Fig. 9

Figure 18. Examples of SAR applications: (a) Interferometry (after [14]); (b) agriculture (after [71]); (c) moving target identification (after [74]); (d) vital sign detector (after [76]).

The use of UAS for interferometry is one of the most challenging research fields. The uncontrolled movement affects the phase information, making it difficult to combine data acquired during different flights. Moreover, the altitude of the UAS can change during the flight, affecting the volumetric phase. The volumetric phase is related to the elevation of the environment under test. In [14], Frey et al. used an external system to generate a DEM and remove the volumetric phase contribution. Luebeck et al. [68] located targets on a horizontal plane. The targets were equipped with a displacement system, and they successfully measured the controlled movements. The digital image correlation can be also used for change monitoring [77–79]. This technique can be used both for compensating the movement of the UAS or for detecting a fast movement of the environment on the image plane.

The use of UAS-borne SAR for agricultural applications is of particular interest. These systems allow for the monitoring of large areas with an elevated periodicity. In [70,71], Oré et al. applied the SAR technique for the monitoring of crops and sugarcane fields. They used the phase information both to measure the differential growth within the field and the total growth over time. Moreira et al. exploited the same equipment for the monitoring of the forest status [72].

Most of the papers regarding SAR applications are related to technical developments and the most used modulation for UAS-borne SAR is FMCW (about 80%), with a small percentage of pulsed radars (about 9%). Figure 19 summarizes the operative bands used

for SAR applications. The C-band is the most used operative band (about 20% of papers regarding SAR application), followed by the L- and W-bands (about 15% each).

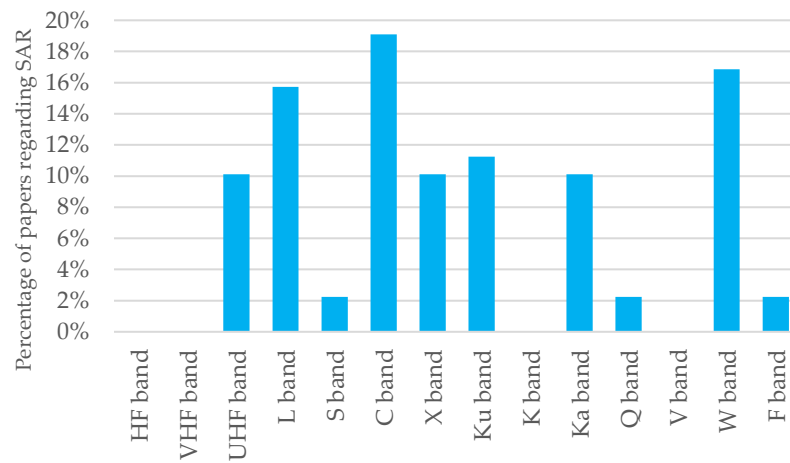


Figure 19. Percentage of papers regarding SAR applications in terms of operative band.

5.2. Ground Penetrating Radar

Some examples of GPR applications are shown in Figure 20: Landmine detection (Figure 20a) [12,29,30,44–47,49,52,80–83], search and rescue operations (Figure 20b) [53,84,85], soil moisture measurement (Figure 20c) [62,86,87]. Furthermore, the UAS-borne GPS is used for snow monitoring [13,26–28,88,89].

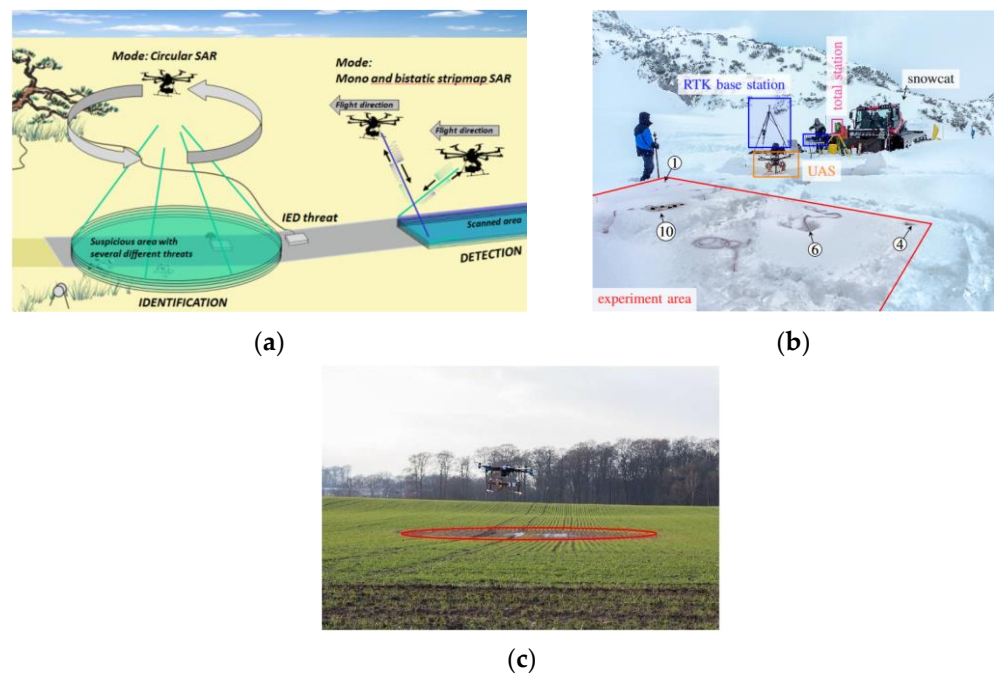


Figure 20. Examples of GPR applications: (a) Landmine detection (after [44]); (b) search and rescue (after [53]); (c) soil moisture (after [62]).

The landmine detection is the main application of UAS-borne GPR with 56% of papers (blue slice in Figure 21) followed by snow monitoring (15%, light blue dotted slice in Figure 21). About 8% of papers are related to search and rescue activities, and 5% to soil moisture application. Furthermore, 9% of papers are equally divided into underground prospection, quarry monitoring, and archaeological applications.

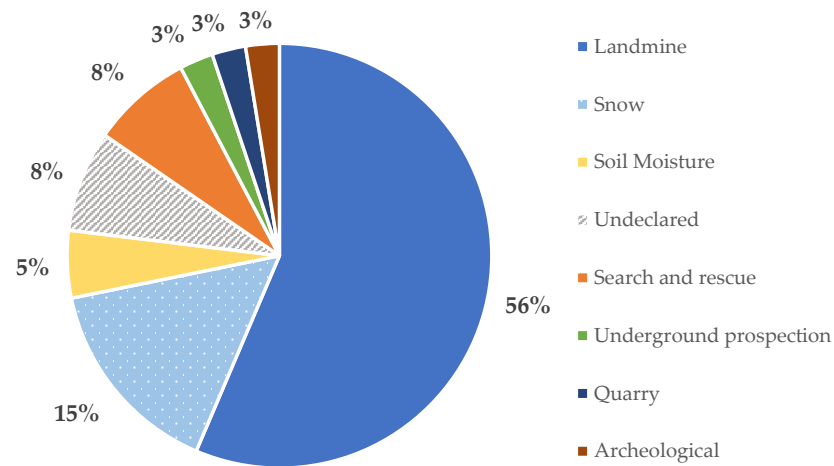


Figure 21. Percentage of papers in terms of specific application in GPR category.

Garcia-Fernandez et al. proposed several equipment for landmine detection and produced about 20% of publications with respect to UAS-borne GPR. They proposed two different systems: The first operated the C-band with helix antennas [90], and the second operated UHF with MIMO Vivaldi antennas [12]. Using the second system, the authors were able to determine the coordinates of a buried object with a single scan. A different approach for landmine detection has been used by Burr et al. [45,47]. Here, the authors designed an L-band MIMO system with two transmitters and two receivers. They used the MIMO capabilities to obtain a digital elevation model [47], and perform polarimetric measurements [45].

Snow monitoring is a key application of GPR. Important characteristics of the snow cover can be retrieved from a radar survey, such as snow depth distribution or snow water equivalent. Using UAS-borne GPR, it is possible to cover large areas with a relative resource efficiency (in terms of time and cost). Jessen et al. used a UHF band pseudo noise-modulated radar for the retrieval of snowpack characteristics [13,26,27]. In [89], Vergnano et al. proposed a C-band radar for the retrieval of snow depth distribution. The results of the survey were compared to other methods and the deviation between these was less than 10%.

In terms of signal modulation, the UAS-borne GPR equipment are equally distributed between pulse and FMCW systems (30% of publications for each of these modulations). The pulse signal is the most common for conventional GPR systems. Many authors adapted conventional equipment for UAS application. On the other hand, many FMCW systems are especially designed for UAS-borne GPR applications. Furthermore, Figure 22 shows the operative bandwidth used for GPR applications.

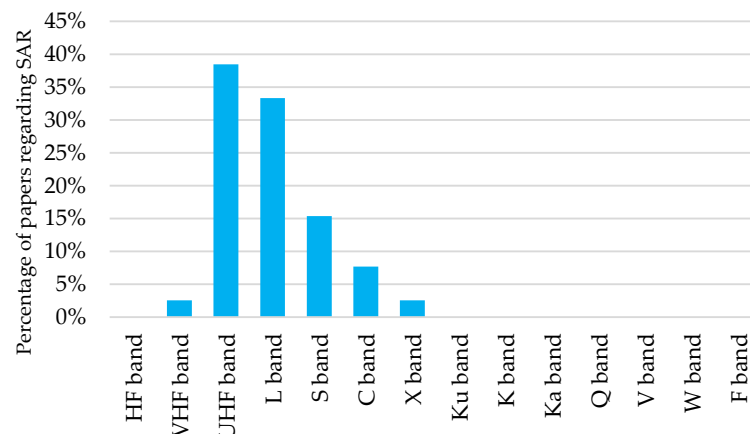


Figure 22. Percentage of papers regarding GPR applications in terms of operative band.

6. Discussion

The technological developments and the applications of UAS-borne radar have been discussed in this review. The review on the state-of-the-art of this technology could be used, both for understanding the trend of radar developments, and for providing the researcher with a possible reading key if they would like to address the UAS-borne radar. From the application results, the scholars could be inspired to develop novel applications. Furthermore, we provided an overview of the main national UAS regulation. This overview, far from being complete, can be used as a future track for the next generation of UAS-borne radars, which must comply with the regulation.

The UAS-borne radar appears to be a few steps behind other payload technologies (optical, multispectral, infrared sensors, etc.) in terms of industrialization. In fact, the UAS-borne radar is a mature technology, even if it is not yet standardized, for example, regard to the radar operative bandwidth.

With respect to the UAS category, the multi-copter will be the most used system in the next future. Indeed, since 2016, the interest in multi-copter systems has increased in terms of fixed-wing systems. To date, the percentage of papers that uses fixed-wing UAS is lower than 10%, while the percentage of papers that uses multi-copter increased by up to 80% (Figure 17). The multi-copters overclass the fixed-wing UAS, thanks to their maneuverability and relative low cost. On the other hand, particular attention should be paid to the MTOW and the autonomy of multi-copters, which are often lower than fixed-wings. Moreover, the multi-copters allow for the planning of automatic routines, for example, they are able to follow a series of waypoints. These routines are currently used in all surveying operations, but they need careful human planning to avoid collisions with possible obstacles. To further automate the routines, the UAS can be equipped by obstacle detection systems based on radars [91–93].

In regard to applications, the UAS has already been successfully used for GPR in many cases. The use of UAS-borne GPR could allow for the monitoring of large areas with little effort in terms of time and cost. Indeed, the UAS-borne GPR can automatically cover large areas by following a pre-generated trajectory, while the terrestrial systems need an operator that can drive the GPR on a scan-by-scan. Currently, the UAS-borne GPR can be employed in dangerous situations, such as landmine detection (50% of papers) or search and rescue purposes (8% of papers), and these will possibly be the main application fields of UAS-borne GPR. Another promising application is the underground utilities survey. With respect to archeological or geochemical surveys, the search for sub-services could be easily carried out by the UAS since these sub-services are often relatively close to the surface.

With respect to SAR applications, the UAS-borne system could bridge the gap between satellite and ground-based systems both for imaging and interferometric purposes. The application in agriculture and for environmental conservation is of particular interest. The UAS-borne SAR could represent an essential tool for smart agriculture (by monitoring the growth of plantation, see Figure 18b) or for wooden conservation. The UAS-borne radar will make it possible and affordable to retrieve crucial information on the ecosystem, about the cover, the biomass value, and the homogeneity of the area.

Nevertheless, the SAR applications could be the real key to the widespread use of UAS-borne radar. In fact, the impressive images retrieved with UAS systems currently compete with those acquired by aerial systems both for the resolution and area covered. In addition, to totally bridge the gap between terrestrial and satellite systems, the UAS-borne SAR must be able to perform interferometric measurements. To date, only a few research groups exploited this possibility, probably since this application is critically affected by the accuracy of pose systems. Indeed, to successfully perform an interferometric measurement, it is necessary to retrace the same path with high accuracy. An improvement of pose systems technology could lead to the exploitation of the full potential of UAS-borne SAR. Moreover, some scholars are currently working on control systems to retrace the same trajectory several times [94]. This approach is complementary to an enhancement of pose

systems, but it allows for the development of automatic routines to scan the same area several times.

In regard to radar modulation, our study identified the FMCW modulation to be the most used and the most promising for a major part of UAS-borne radar applications (about 63% of papers). Nevertheless, some specific applications may benefit from pulse radars which may be more suitable. This is the case for GPR applications, in which the UAS could be equipped with a pulse radar adapted from conventional terrestrial radars.

For the operative band, the most used are UHF, L-, C-, and W-bands. Specifically, UHF and L-bands are frequently used (about 72% of papers) for GPR applications, while C- and W-bands (about 34% of papers) for SAR. For GPR applications, the reason is clear: The lower the band, the greater the penetration of depth.

The use of C-band instruments for SAR interferometry applications is motivated by the fact that the C-band signal is rather insensitive to errors in trajectory measurements. Therefore, the use of this band could allow for overcoming one of the main problems of SAR interferometry. On the other hand, with W-band systems, it is possible to perform high-resolution SAR mapping (the higher the band, the larger the bandwidth, the better the resolution). In this case, the lack of information on the UAS trajectory overcomes the problem using motion compensation techniques that involve autofocusing algorithms.

7. Conclusions

The UAS-borne radar appears to be a mature technology for the global market. However, national regulations could limit the use of UAS-borne radars. Of note, the maximum take-off weight is a discriminating parameter in many countries, which places the greatest limitations on systems use. Moreover, the absence of homogeneous regulations in most of the countries do not permit the development of a unique solution, and represents a challenge for the developer. Furthermore, most of the current regulations do not allow for the use of UAS without a line-of-sight or even remotely. This part of the regulations reduces the potentiality of the UAS-borne radar in a few scenarios, while the autonomous operations are particularly useful in many important applications (for example, in mines).

Regulators should consider these applications and adopt less restrictive regulations, while maintaining high safety standards for flight systems.

In conclusion, the deployment of radars might be facilitated by improving the technological level of UAVs, especially in regard to positioning and inertial systems, flight autonomy, mass of the UAS with respect to the payload, and automatic/autonomous routine.

Author Contributions: Conceptualization, L.M. and M.P.; validation, L.M.; formal analysis, L.M.; investigation, L.M.; data curation, L.M.; writing—original draft preparation, L.M.; writing—review and editing, A.B. and M.P.; supervision, M.P. All authors have read and agreed to the published version of the manuscript.

Funding: This research received no external funding.

Data Availability Statement: Not applicable.

Conflicts of Interest: The authors declare no conflict of interest.

References

1. Zhang, C.; Kovacs, J.M. The Application of Small Unmanned Aerial Systems for Precision Agriculture: A Review. *Precis. Agric.* **2012**, *13*, 693–712. [[CrossRef](#)]
2. Manfreda, S.; McCabe, M.F.; Miller, P.E.; Lucas, R.; Pajuelo Madrigal, V.; Mallinis, G.; Ben Dor, E.; Helman, D.; Estes, L.; Ciraolo, G.; et al. On the Use of Unmanned Aerial Systems for Environmental Monitoring. *Remote Sens.* **2018**, *10*, 641. [[CrossRef](#)]
3. Wang, D.; Shao, Q.; Yue, H. Surveying Wild Animals from Satellites, Manned Aircraft and Unmanned Aerial Systems (UASs): A Review. *Remote Sens.* **2019**, *11*, 1308. [[CrossRef](#)]
4. Hardin, P.J.; Lulla, V.; Jensen, R.R.; Jensen, J.R. Small Unmanned Aerial Systems (SUAS) for Environmental Remote Sensing: Challenges and Opportunities Revisited. *GIScience Remote Sens.* **2019**, *56*, 309–322. [[CrossRef](#)]
5. Adamopoulos, E.; Rinaudo, F. UAS-Based Archaeological Remote Sensing: Review, Meta-Analysis and State-of-the-Art. *Drones* **2020**, *4*, 46. [[CrossRef](#)]

6. Poley, L.G.; McDermid, G.J. A Systematic Review of the Factors Influencing the Estimation of Vegetation Aboveground Biomass Using Unmanned Aerial Systems. *Remote Sens.* **2020**, *12*, 1052. [CrossRef]
7. Vélez-Nicolás, M.; García-López, S.; Barbero, L.; Ruiz-Ortiz, V.; Sánchez-Bellón, Á. Applications of Unmanned Aerial Systems (UASs) in Hydrology: A Review. *Remote Sens.* **2021**, *13*, 1359. [CrossRef]
8. Colomina, I.; Molina, P. Unmanned Aerial Systems for Photogrammetry and Remote Sensing: A Review. *ISPRS J. Photogramm. Remote Sens.* **2014**, *92*, 79–97. [CrossRef]
9. Pieraccini, M.; Miccinesi, L. Ground-Based Radar Interferometry: A Bibliographic Review. *Remote Sens.* **2019**, *11*, 1029. [CrossRef]
10. Cruz, H.; Véstias, M.; Monteiro, J.; Neto, H.; Duarte, R.P. A Review of Synthetic-Aperture Radar Image Formation Algorithms and Implementations: A Computational Perspective. *Remote Sens.* **2022**, *14*, 1258. [CrossRef]
11. Zaugg, E.C.; Hudson, D.L.; Long, D.G. The BYU MSAR: A Small, Student-Built SAR for UAV Operation. In Proceedings of the 2006 IEEE International Symposium on Geoscience and Remote Sensing, Denver, CO, USA, 31 July–2 August 2006; pp. 411–414.
12. García-Fernández, M.; López, Y.Á.; Andrés, F.L.-H. Airborne Multi-Channel Ground Penetrating Radar for Improvised Explosive Devices and Landmine Detection. *IEEE Access* **2020**, *8*, 165927–165943. [CrossRef]
13. Jenssen, R.O.R.; Eckerstorfer, M.; Jacobsen, S. Drone-Mounted Ultrawideband Radar for Retrieval of Snowpack Properties. *IEEE Trans. Instrum. Meas.* **2020**, *69*, 221–230. [CrossRef]
14. Frey, O.; Werner, C.L.; Coscione, R. Car-Borne and UAV-Borne Mobile Mapping of Surface Displacements with a Compact Repeat-Pass Interferometric SAR System at L-Band. In Proceedings of the IGARSS 2019–2019 IEEE International Geoscience and Remote Sensing Symposium, Yokohama, Japan, 28 July–2 August 2019; pp. 274–277.
15. Chen, Y.; Hakala, T.; Karjalainen, M.; Feng, Z.; Tang, J.; Litkey, P.; Kukko, A.; Jaakkola, A.; Hyypä, J. UAV-Borne Profiling Radar for Forest Research. *Remote Sens.* **2017**, *9*, 58. [CrossRef]
16. Zotero | Your Personal Research Assistant. Available online: <https://www.zotero.org/start> (accessed on 8 April 2019).
17. Drone Laws [By Countries, States, Cities]—[Updated 13 July 2022]. Available online: <https://drone-laws.com/> (accessed on 20 September 2022).
18. Vesecky, J.F.; Cornwall, J.M. Integrated Design of Synthetic Aperture Radars for Unmanned Aircraft. In Proceedings of the IGARSS '96. 1996 International Geoscience and Remote Sensing Symposium, Lincoln, NE, USA, 31 May 1996; Volume 4, pp. 2347–2348.
19. Civil Drones (Unmanned Aircraft). Available online: <https://www.easa.europa.eu/domains/civil-drones> (accessed on 25 July 2022).
20. Drone Laws in China [Updated 13 July 2022]. Available online: <https://drone-laws.com/drone-laws-in-china/> (accessed on 25 July 2022).
21. Drone Laws in India [Updated 14 July 2022]. Available online: <https://drone-laws.com/drone-laws-in-india/> (accessed on 25 July 2022).
22. Remotely Piloted Aircraft System (RPAS). Directorate General of Civil Aviation, India. Available online: <https://www.dgca.gov.in/digigov-portal/?page=jsp/dgca/InventoryList/headerblock/drones/RPAS.html> (accessed on 25 July 2022).
23. Canada, T. Flying Your Drone Safely and Legally. Available online: <https://tc.canada.ca/en/aviation/drone-safety/learn-rules-you-fly-your-drone/flying-your-drone-safely-legally> (accessed on 2 August 2022).
24. Unmanned Aircraft Systems (UAS) | Federal Aviation Administration. Available online: <https://www.faa.gov/uas> (accessed on 25 July 2022).
25. Pieraccini, M. Noise Performance Comparison Between Continuous Wave and Stroboscopic Pulse Ground Penetrating Radar. *IEEE Geosci. Remote Sens. Lett.* **2018**, *15*, 222–226. [CrossRef]
26. Jenssen, R.O.R.; Jacobsen, S. Drone-Mounted UWB Snow Radar: Technical Improvements and Field Results. *J. Electromagn. Waves Appl.* **2020**, *34*, 1930–1954. [CrossRef]
27. Jenssen, R.O.R.; Jacobsen, S.K. Measurement of Snow Water Equivalent Using Drone-Mounted Ultra-Wide-Band Radar. *Remote Sens.* **2021**, *13*, 2610. [CrossRef]
28. Patel, M.; Ferguson, P. Tracking and Estimation of a Swaying Payload Using a LiDAR and an Extended Kalman Filter. In Proceedings of the 2021 IEEE International Symposium on Robotic and Sensors Environments (ROSE), Piscataway, NJ, USA, 28–29 October 2021; pp. 1–7.
29. Garcia-Fernandez, M.; Alvarez-Lopez, Y.; Heras, F.L.; Gonzalez-Valdes, B.; Rodriguez-Vaqueiro, Y.; Pino, A.; Arboleya-Arboleya, A. GPR System Onboard a UAV for Non-Invasive Detection of Buried Objects. In Proceedings of the 2018 IEEE International Symposium on Antennas and Propagation & USNC/URSI National Radio Science Meeting, Boston, MA, USA, 8–13 July 2018; pp. 1967–1968.
30. Schartel, M.; Prakasan, K.; Hügl, P.; Burr, R.; Mayer, W.; Waldschmidt, C. A Multicopter-Based Focusing Method for Ground Penetrating Synthetic Aperture Radars. In Proceedings of the IGARSS 2018–2018 IEEE International Geoscience and Remote Sensing Symposium, Valencia, Spain, 22–27 July 2018; pp. 5420–5423.
31. Ding, M.-L.; Ding, C.-B.; Tang, L.; Wang, X.-M.; Qu, J.-M.; Wu, R. A W-Band 3-D Integrated Mini-SAR System With High Imaging Resolution on UAV Platform. *IEEE Access* **2020**, *8*, 113601–113609. [CrossRef]
32. Ding, M.; Liang, X.; Tang, L.; Wen, Z.; Wang, X.; Wang, Y. Micro FMCW SAR with High Resolution for Mini UAV. In Proceedings of the 2018 International Conference on Microwave and Millimeter Wave Technology (ICMMT), Chengdu, China, 7–11 May 2018; pp. 1–3.

33. Wang, Y.; Lou, L.; Chen, B.; Zhang, Y.; Tang, K.; Qiu, L.; Liu, S.; Zheng, Y. A 260-MW Ku-Band FMCW Transceiver for Synthetic Aperture Radar Sensor With 1.48-GHz Bandwidth in 65-Nm CMOS Technology. *IEEE Trans. Microw. Theory Tech.* **2017**, *65*, 4385–4399. [[CrossRef](#)]
34. Ludeno, G.; Catapano, I.; Renga, A.; Vetrella, A.R.; Fasano, G.; Soldovieri, F. Assessment of a Micro-UAV System for Microwave Tomography Radar Imaging. *Remote Sens. Environ.* **2018**, *212*, 90–102. [[CrossRef](#)]
35. Fasano, G.; Renga, A.; Vetrella, A.R.; Ludeno, G.; Catapano, I.; Soldovieri, F. Proof of Concept of Micro-UAV-Based Radar Imaging. In Proceedings of the 2017 International Conference on Unmanned Aircraft Systems (ICUAS), Miami, FL, USA, 13–16 June 2017; pp. 1316–1323.
36. Esposito, G.; Noviello, C.; Soldovieri, F.; Catapano, I.; Fasano, G.; Gagliarde, G.; Luisi, G.; Saccoccio, F. The UAV Radar Imaging Prototype Developed in the Frame of the VESTA Project. In Proceedings of the 2020 IEEE Radar Conference (RadarConf20), Florence, Italy, 21–25 September 2020; pp. 1–5.
37. Ye, E.; Shaker, G.; Melek, W. Lightweight Low-Cost UAV Radar Terrain Mapping. In Proceedings of the 2019 13th European Conference on Antennas and Propagation (EuCAP), Krakow, Poland, 31 March–5 April 2019; pp. 1–5.
38. Pieraccini, M.; Miccinesi, L. ArcSAR: Theory, Simulations, and Experimental Verification. *IEEE Trans. Microw. Theory Tech.* **2017**, *65*, 293–301. [[CrossRef](#)]
39. Schartel, M.; Bähnmann, R.; Burr, R.; Mayer, W.; Waldschmidt, C. Position Acquisition for a Multicopter-Based Synthetic Aperture Radar. In Proceedings of the 2019 20th International Radar Symposium (IRS), Ulm, Germany, 26–28 June 2019; pp. 1–7.
40. Pieraccini, M.; Miccinesi, L. ArcSAR for Detecting Target Elevation. *Electron. Lett.* **2016**, *52*, 1559–1561. [[CrossRef](#)]
41. Viviani, F.; Michelini, A.; Mayer, L.; Conni, F. IBIS-ArcSAR: An Innovative Ground-Based SAR System for Slope Monitoring. In Proceedings of the IGARSS 2018–2018 IEEE International Geoscience and Remote Sensing Symposium, Valencia, Spain, 22–27 July 2018; pp. 1348–1351.
42. Pieraccini, M.; Miccinesi, L. RotoSAR for Monitoring Bridges. In Proceedings of the European Microwave Week 2017: “A Prime Year for a Prime Event”, EuMW 2017—Conference Proceedings; 14th European Microwave Conference, EURAD 2017, Nuremberg, Germany, 11–13 October 2018; Volume 2018, pp. 311–314.
43. Bekar, A.; Antoniou, M.; Baker, C.J. Low-Cost, High-Resolution, Drone-Borne SAR Imaging. *IEEE Trans. Geosci. Remote Sens.* **2022**, *60*, 1–11. [[CrossRef](#)]
44. Engel, M.; Heinzl, A.; Schreiber, E.; Dill, S.; Peichl, M. Recent Results of a UAV-Based Synthetic Aperture Radar for Remote Sensing Applications. In Proceedings of the EUSAR 2021; 13th European Conference on Synthetic Aperture Radar, Online, 29 March–1 April 2021; pp. 1–5.
45. Burr, R.; Schartel, M.; Mayer, W.; Walter, T.; Waldschmidt, C. Uav-Based Polarimetric Synthetic Aperture Radar for Mine Detection. In Proceedings of the IGARSS 2019–2019 IEEE International Geoscience and Remote Sensing Symposium, Yokohama, Japan, 28 July–2 August 2019; pp. 9208–9211.
46. Almutiry, M. UAV Tomographic Synthetic Aperture Radar for Landmine Detection. *Eng. Technol. Appl. Sci. Res.* **2020**, *10*, 5933–5939. [[CrossRef](#)]
47. Burr, R.; Schartel, M.; Grathwohl, A.; Mayer, W.; Walter, T.; Waldschmidt, C. UAV-Borne FMCW InSAR for Focusing Buried Objects. *IEEE Geosci. Remote Sens. Lett.* **2022**, *19*, 1–5. [[CrossRef](#)]
48. Burr, R.; Schartel, M.; Mayer, W.; Walter, T.; Waldschmidt, C. Lightweight Broadband Antennas for UAV Based GPR Sensors. In Proceedings of the 2018 15th European Radar Conference (EuRAD), Madrid, Spain, 26–28 September 2018; pp. 245–248.
49. Schartel, M.; Burr, R.; Mayer, W.; Docci, N.; Waldschmidt, C. UAV-Based Ground Penetrating Synthetic Aperture Radar. In Proceedings of the 2018 IEEE MTT-S International Conference on Microwaves for Intelligent Mobility (ICMIM), Munich, Germany, 16–18 April 2018; pp. 1–4.
50. Garcia-Fernandez, M.; Alvarez-Lopez, Y.; Heras, F.L. 3D-SAR Processing of UAV-Mounted GPR Measurements: Dealing with Non-Uniform Sampling. In Proceedings of the 2020 14th European Conference on Antennas and Propagation (EuCAP), Copenhagen, Denmark, 15–20 March 2020; pp. 1–5.
51. Garcia-Fernandez, M.; Alvarez-Lopez, Y.; Las Heras, F. Autonomous Airborne 3D SAR Imaging System for Subsurface Sensing: UWB-GPR on Board a UAV for Landmine and IED Detection. *Remote Sens.* **2019**, *11*, 2357. [[CrossRef](#)]
52. García-Fernández, M.; Álvarez-Narciandi, G.; López, Y.Á.; Andrés, F.L.-H. SAFEDRONE Project: Development of a UAV-Based High-Resolution GPR System for IED Detection. In Proceedings of the 2022 16th European Conference on Antennas and Propagation (EuCAP), Madrid, Spain, 27 March–1 April 2022; pp. 1–5.
53. Grathwohl, A.; Hinz, P.; Burr, R.; Steiner, M.; Waldschmidt, C. Experimental Study on the Detection of Avalanche Victims Using an Airborne Ground Penetrating Synthetic Aperture Radar. In Proceedings of the 2021 IEEE Radar Conference (RadarConf21), Atlanta, GA, USA, 7–14 May 2021; pp. 1–6.
54. Lort, M.; Aguasca, A.; López-Martínez, C.; Marín, T.M. Initial Evaluation of SAR Capabilities in UAV Multicopter Platforms. *IEEE J. Sel. Top. Appl. Earth Obs. Remote Sens.* **2018**, *11*, 127–140. [[CrossRef](#)]
55. Wahl, D.E.; Eichel, P.H.; Ghiglia, D.C.; Jakowatz, C.V. Phase Gradient Autofocus—a Robust Tool for High Resolution SAR Phase Correction. *IEEE Trans. Aerosp. Electron. Syst.* **1994**, *30*, 827–835. [[CrossRef](#)]
56. Saeedi, J.; Faez, K. A Back-Projection Autofocus Algorithm Based on Flight Trajectory Optimization for Synthetic Aperture Radar Imaging. *Multidimens. Syst. Signal Process.* **2016**, *27*, 411–431. [[CrossRef](#)]

57. Ding, Z.; Zhu, K.; Zhang, T.; Li, L.; Wang, Y.; Wang, G.; Gao, Y.; Wei, Y.; Zeng, T. An Autofocus Back Projection Algorithm for GEO SAR Based on Minimum Entropy. *IEEE Trans. Geosci. Remote Sens.* **2022**, *60*, 1–14. [[CrossRef](#)]
58. Ding, Z.; Li, L.; Wang, Y.; Zhang, T.; Gao, W.; Zhu, K.; Zeng, T.; Yao, D. An Autofocus Approach for UAV-Based Ultrawideband Ultrawidebeam SAR Data With Frequency-Dependent and 2-D Space-Variant Motion Errors. *IEEE Trans. Geosci. Remote Sens.* **2022**, *60*, 1–18. [[CrossRef](#)]
59. Liu, W.; Feng, H.; Lu, Y. Ka-Band Drone SAR Flying without GPS. In Proceedings of the 2021 7th Asia-Pacific Conference on Synthetic Aperture Radar (APSAR), Bali, Indonesia, 1–3 November 2021; pp. 1–4.
60. Zaugg, E.; Edwards, M.; Long, D.; Stringham, C. Developments in Compact High-Performance Synthetic Aperture Radar Systems for Use on Small Unmanned Aircraft. In Proceedings of the 2011 Aerospace Conference, Big Sky, MT, USA, 5–12 March 2011; pp. 1–14.
61. Tetuko, S.S.J.; Koo, V.C.; Lim, T.S.; Kawai, T.; Ebinuma, T.; Izumi, Y.; Baharuddin, M.Z.; Gao, S.; Ito, K. Development of Circularly Polarized Synthetic Aperture Radar On-Board UAV JX-1. *Int. J. Remote Sens.* **2017**, *38*, 2745–2756. [[CrossRef](#)]
62. Wu, K.; Rodriguez, G.A.; Zajc, M.; Jacquemin, E.; Clément, M.; De Coster, A.; Lambot, S. A New Drone-Borne GPR for Soil Moisture Mapping. *Remote Sens. Environ.* **2019**, *235*, 111456. [[CrossRef](#)]
63. Essen, H.; Johannes, W.; Stanko, S.; Sommer, R.; Wahlen, A.; Wilcke, J. High Resolution W-Band UAV SAR. In Proceedings of the 2012 IEEE International Geoscience and Remote Sensing Symposium, Munich, Germany, 22–27 July 2012; pp. 5033–5036.
64. Kim, J.; Kim, S.; Lee, W.; Shin, S.; Choi, Y.; Ka, M.-H. Design and Implementation of Compact 77 GHz Synthetic Aperture Radar for Drone Based Applications. In Proceedings of the 2019 6th Asia-Pacific Conference on Synthetic Aperture Radar (APSAR), Xiamen, China, 26–29 November 2019; pp. 1–5.
65. Moreira, L.; Castro, F.; Góes, J.A.; Bins, L.; Teruel, B.; Fracarolli, J.; Castro, V.; Alcântara, M.; Oré, G.; Luebeck, D.; et al. A Drone-Borne Multiband DInSAR: Results and Applications. In Proceedings of the 2019 IEEE Radar Conference (RadarConf), Boston, MA, USA, 22–26 April 2019; pp. 1–6.
66. Deguchi, T.; Sugiyama, T.; Kishimoto, M. R&D of drone-borne SAR system. *Int. Arch. Photogramm. Remote Sens. Spat. Inf. Sci.* **2019**, *XLII-2/W13*, 263–267. [[CrossRef](#)]
67. Deguchi, T.; Sugiyama, T.; Kishimoto, M. Development of SAR System Installable on a Drone. In Proceedings of the EUSAR 2021; 13th European Conference on Synthetic Aperture Radar, Online, 29 March–1 April 2021; pp. 1–3.
68. Luebeck, D.; Wimmer, C.; Moreira, L.F.; Alcântara, M.; Oré, G.; Góes, J.A.; Oliveira, L.P.; Teruel, B.; Bins, L.S.; Gabrielli, L.H.; et al. Drone-Borne Differential SAR Interferometry. *Remote Sens.* **2020**, *12*, 778. [[CrossRef](#)]
69. Lv, Z.; Li, F.; Qiu, X.; Ding, C. Effects of Motion Compensation Residual Error and Polarization Distortion on UAV-Borne PolInSAR. *Remote Sens.* **2021**, *13*, 618. [[CrossRef](#)]
70. Oré, G.; Alcântara, M.S.; Góes, J.A.; Teruel, B.; Oliveira, L.P.; Yepes, J.; Castro, V.; Bins, L.S.; Castro, F.; Luebeck, D.; et al. Predicting Sugarcane Harvest Date and Productivity with a Drone-Borne Tri-Band SAR. *Remote Sens.* **2022**, *14*, 1734. [[CrossRef](#)]
71. Oré, G.; Alcântara, M.S.; Góes, J.A.; Oliveira, L.P.; Yepes, J.; Teruel, B.; Castro, V.; Bins, L.S.; Castro, F.; Luebeck, D.; et al. Crop Growth Monitoring with Drone-Borne DInSAR. *Remote Sens.* **2020**, *12*, 615. [[CrossRef](#)]
72. Moreira, L.; Lübeck, D.; Wimmer, C.; Castro, F.; Góes, J.A.; Castro, V.; Alcântara, M.; Oré, G.; Oliveira, L.P.; Bins, L.; et al. Drone-Borne P-Band Single-Pass InSAR. In Proceedings of the 2020 IEEE Radar Conference (RadarConf20), Florence, Italy, 21–25 September 2020; pp. 1–6.
73. Hawkins, B.; Anderson, M.; Prager, S.; Chung, S.-I.; Lavalle, M. Experiments with Small UAS to Support SAR Tomographic Mission Formulation. In Proceedings of the 2021 IEEE International Geoscience and Remote Sensing Symposium IGARSS, Brussels, Belgium, 11–16 July 2021; pp. 643–646.
74. Gromek, D.; Samczynski, P.; Kulpa, K.; Cruz, G.C.S.; Oliveira, T.M.M.; Félix, L.F.S.; Gonçalves, P.A.V.; Silva, C.M.B.P.; Santos, A.L.C.; Morgado, J.A.P. C-Band SAR Radar Trials Using UAV Platform: Experimental Results of SAR System Integration on a UAV Carrier. In Proceedings of the 2016 17th International Radar Symposium (IRS), Krakow, Poland, 10–12 May 2016; pp. 1–5.
75. Hu, X.; Ma, C.; Hu, R.; Yeo, T.S. Imaging for Small UAV-Borne FMCW SAR. *Sensors* **2019**, *19*, 87. [[CrossRef](#)]
76. Yan, J.; Peng, Z.; Hong, H.; Chu, H.; Zhu, X.; Li, C. Vital-SAR-Imaging With a Drone-Based Hybrid Radar System. *IEEE Trans. Microw. Theory Tech.* **2018**, *66*, 5852–5862. [[CrossRef](#)]
77. Wu, Y.; Li, J.; Yuan, Y.; Qin, A.K.; Miao, Q.-G.; Gong, M.-G. Commonality Autoencoder: Learning Common Features for Change Detection From Heterogeneous Images. *IEEE Trans. Neural Netw. Learn. Syst.* **2022**, *33*, 4257–4270. [[CrossRef](#)]
78. Wu, Y.; Xiao, Z.; Liu, S.; Miao, Q.; Ma, W.; Gong, M.; Xie, F.; Zhang, Y. A Two-Step Method for Remote Sensing Images Registration Based on Local and Global Constraints. *IEEE J. Sel. Top. Appl. Earth Obs. Remote Sens.* **2021**, *14*, 5194–5206. [[CrossRef](#)]
79. Caporossi, P.; Mazzanti, P.; Bozzano, F. Digital Image Correlation (DIC) Analysis of the 3 December 2013 Montescaglioso Landslide (Basilicata, Southern Italy): Results from a Multi-Dataset Investigation. *ISPRS Int. J. Geo-Inf.* **2018**, *7*, 372. [[CrossRef](#)]
80. Sipos, D.; Planinsic, P.; Gleich, D. On Drone Ground Penetrating Radar for Landmine Detection. In Proceedings of the 2017 First International Conference on Landmine: Detection, Clearance and Legislations (LDCL), Beirut, Lebanon, 26–28 April 2017; pp. 1–4.
81. Dill, S.; Schreiber, E.; Engel, M.; Heinzl, A.; Peichl, M. A Drone Carried Multichannel Synthetic Aperture Radar for Advanced Buried Object Detection. In Proceedings of the 2019 IEEE Radar Conference (RadarConf), Boston, MA, USA, 22–26 April 2019; pp. 1–6.

82. Garcia-Fernandez, M.; Morgenthaler, A.; Alvarez-Lopez, Y.; Las Heras, F.; Rappaport, C. Bistatic Landmine and IED Detection Combining Vehicle and Drone Mounted GPR Sensors. *Remote Sens.* **2019**, *11*, 2299. [[CrossRef](#)]
83. Garcia-Fernandez, M.; Alvarez-Lopez, Y.; Las Heras, F.; Morgenthaler, A.; Rappaport, C. Analysis of Multistatic Vehicle-Drone Ground Penetrating Radar Configurations for Mine Detection. In Proceedings of the 2019 IEEE International Symposium on Antennas and Propagation and USNC-URSI Radio Science Meeting, Atlanta, GA, USA, 7–12 July 2019; pp. 1637–1638.
84. Rong, Y.; Gutierrez, R.; Mishra, K.V.; Bliss, D.W. Noncontact Vital Sign Detection With UAV-Borne Radars: An Overview of Recent Advances. *IEEE Veh. Technol. Mag.* **2021**, *16*, 118–128. [[CrossRef](#)]
85. Chandra, M.; Tanzi, T.J. Drone-Borne GPR Design: Propagation Issues. *Comptes Rendus Phys.* **2018**, *19*, 72–84. [[CrossRef](#)]
86. Simpson, C.D.; Kolpuke, S.; Awasthi, A.K.; Luong, T.; Memari, S.; Yan, S.; Taylor, R.; Larson, J.; Clement, P. Development of A UAS-Based Ultra-Wideband Radar for Fine-Resolution Soil Moisture Measurements. In Proceedings of the 2021 IEEE Radar Conference (RadarConf21), San Antonio, TX, USA, 1–5 May 2021; pp. 1–4.
87. Pantoja, J.J.; Vega, F.; Prado, L.; Yang, Q.; AlAli, B.; Kasmi, C.; Moreira, L.; Lübeck, D.; Wimmer, C. Drone-Borne Synthetic Aperture Radar for GPR Applications: Buried Pipe Inspection. In Proceedings of the 2022 3rd URSI Atlantic and Asia Pacific Radio Science Meeting (AT-AP-RASC), Gran Canaria, Spain, 29 May–3 June 2022; pp. 1–2.
88. Tan, A.; Eccleston, K.; Platt, I.; Woodhead, I.; Rack, W.; McCulloch, J. The Design of a UAV Mounted Snow Depth Radar: Results of Measurements on Antarctic Sea Ice. In Proceedings of the 2017 IEEE Conference on Antenna Measurements & Applications (CAMA), Tsukuba, Japan, 4–6 December 2017; pp. 316–319.
89. Vergnano, A.; Franco, D.; Godio, A. Drone-Borne Ground-Penetrating Radar for Snow Cover Mapping. *Remote Sens.* **2022**, *14*, 1763. [[CrossRef](#)]
90. García Fernández, M.; Álvarez López, Y.; Arboleya Arboleya, A.; González Valdés, B.; Rodríguez Vaqueiro, Y.; Las-Heras Andrés, F.; Pino García, A. Synthetic Aperture Radar Imaging System for Landmine Detection Using a Ground Penetrating Radar on Board a Unmanned Aerial Vehicle. *IEEE Access* **2018**, *6*, 45100–45112. [[CrossRef](#)]
91. UAV Collision Avoidance Radar_Nanoradar-Accurate Measure Intelligent Sense. Available online: <http://en.nanoradar.cn/Article/detail/id/287.html> (accessed on 23 September 2022).
92. Miccinesi, L.; Bigazzi, L.; Consumi, T.; Pieraccini, M.; Beni, A.; Boni, E.; Basso, M. Geo-Referenced Mapping through an Anti-Collision Radar Aboard an Unmanned Aerial System. *Drones* **2022**, *6*, 72. [[CrossRef](#)]
93. Matrice 300 RTK. Available online: <https://www.dji.com/matrice-300?site=brandsite&from=nav> (accessed on 23 September 2022).
94. Bigazzi, L.; Basso, M.; Boni, E.; Innocenti, G.; Pieraccini, M. A Multilevel Architecture for Autonomous UAVs. *Drones* **2021**, *5*, 55. [[CrossRef](#)]